Journal of Applied Mechanics and Technical Physics, Vol. 41, No. 3, 2000

BEHAVIOR OF METALLIC SHAPED-CHARGE JETS WITH PASSAGE OF A PULSED ELECTRIC CURRENT THROUGH THEM

G. A. Shvetsov, A. D. Matrosov, A. V. Babkin,[1] S. V. Ladov,[1] and S. V. Fedorov[1]

UDC 623.4.082.6+532.52+533.95

The paper reports results of experimental and numerical studies of the disruption of metallic shaped-charge jets by passage of a pulsed electric current through them. Experimental results are presented in the form of x-ray photographs of shaped-charge jets with and without a current and tables of penetration depths in targets. Numerical simulation of the disruption of shaped-charge jets with a current is performed for three possible mechanisms of disruption (development of MHD *instability of shaped-charge jets, volume fracture, and simultaneous development of* MHD *instability and volume fracture). Numerical and experimental results are compared.*

Introduction. In recent years, several papers on the effect of a pulsed electric current on metallic shaped-charge jets (SCJ) have been published (see, for example, [1–3]). It has been shown experimentally and theoretically that the action of an electric current leads to a change in the jet "structure" and a decrease in the time of jet disruption, which, in turn, results in a severalfold decrease in penetration into the target. This effect is of great practical interest. The mechanisms of SCJ disruption by a pulsed current and their effect on the SCJ penetration into targets have been studied inadequately. The present paper reports results of experimental and numerical studies of SCJ disruption by an electric current.

Numerical simulation was performed for the following three possible mechanisms of disruption: (a) development of MHD instability of SCJ; (b) volume fracture; (c) simultaneous development of MHD instability and volume fracture.

The processes of formation, stretching, and penetration of SCJ with and without an electric current were simulated numerically.

Results of the numerical simulation were compared with experimental data on the SCJ structure and penetration into steel and aluminum targets for various electric-pulse parameters.

Diagram of Experiments. Diagrams of the experiments are given in Fig. 1a and b, where 1 is the shaped charge (SC), 2 is the electromagnetic-energy source, 3 are the electrodes, 4 are the inductive probes for measuring the current and the discharge-current derivative, 5 are the sites of radiography of the SCJ parameters (in an aluminum target and in free flight), and 6 is the target. In the diagram in Fig. 1b, unlike in the diagram of Fig. 1a, the current can flow in the jet during jet penetration into the target. The cavern producing the target can act as an inverse current lead. In this case, the time during which the current acts on a jet element is much larger than that in the diagram shown in Fig. 1a. The experiments were performed with SC of 50- and 100-mm diameters and steel and aluminum targets. The energy source in the experiments was a capacitor bank with charging voltage of up to 5 kV and a capacitance of up to 20 mF. The current

Lavrent'ev Institute of Hydrodynamics, Siberian Division, Russian Academy of Sciences, Novosibirsk 630090. [1]Bauman Moscow State Technical University, Moscow 107005. Translated from Prikladnaya Mekhanika i Tekhnicheskaya Fizika, Vol. 41, No. 3, pp. 19–25, May–June, 2000. Original article submitted February 22, 1999.

 0021-8944/00/4103-0394 $25.00

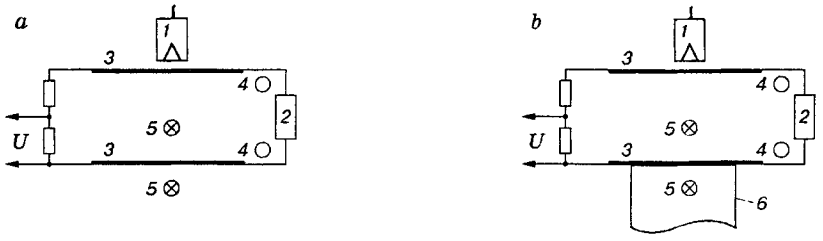

Fig. 1

began to flow through the SCJ from the moment the electrodes were closed by the jet. In the experiments, we changed the current, the discharge-current derivative (100–500 kA and $3 \cdot 10^9$–10^{11} A/sec), the electric-pulse duration, the time of action on the various jet elements, and other parameters. Radiography of the SCJ was performed in free flight and in the target (aluminum). The effect of the electric current on the SCJ penetration into the target was also studied.

Experimental Results. Figure 2 gives x-ray photographs of two experiments with an aluminum target performed according to the diagram shown in Fig. 1b for SC of 50-mm diameter at $t = 52.5$ μsec [Fig. 2a refers to the experiment without a current; Fig. 2b shows the experiment with a current (450 kA)]. It is evident that in the experiment with a current, the jet broke up into separate fragments. The breakup took place inside the cavern.

Figure 3a and c shows x-ray photographs of the jet with and without a current, respectively, at $t = 52.5$ μsec. The experiments were performed with 50-mm-diameter SC according to the diagram shown in Fig. 1a. Figure 3c scales-up the SCJ fragment before the lower electrode given in Fig. 3b. The x-ray photographs show the formation and development of necks. After passing the lower electrode, the jet breaks up into separate fragments whose axial dimensions are approximately equal to 1–3 jet diameters. The fragments expand in the radial direction, reaching 5–10 jet diameters in the same cross sections as in the experiments without a current. Figure 4 gives x-ray photographs of the jets from SC of 100-mm diameter at $t = 108.5$ μsec (Fig. 4a refers to the experiment without a current and Fig. 4b refers to the experiment with a current). The SCJ disruption patterns for the charges of 50- and 100-mm diameters are similar (see Figs. 2–4).

From the x-ray photographs it can be seen that the disruption is accompanied by development of MHD instability and volume fracture of the SCJ material after the jet passes the lower electrode. An analysis of the x-ray photographs shows that the number of necks on the jet without a current is approximately equal to the number of fragments in experiments with a current.

The SCJ in the target (see Fig. 2b) broke up into separate fragments later than the jet in the experiment without a target (see Fig. 3). In the target, the SCJ practically does not undergo volume fracture at the same current strength.

Figures 2 and 3 clearly show disk fragments of the SCJ after disruption.

The disruption of the SCJ by passage of an electric current leads to a severalfold decrease in the penetration depth in the target. This process can be controlled by changing the amplitude of the current, the current rise time, and the electric-pulse duration.

In the experiments with a 50-mm diameter SC, current instability developed and the jet penetration began to decrease if the current and the current derivative exceeded 10^5 A and $3 \cdot 10^9$ A/sec, respectively.

Simulation of the Effect of an Electric Current on Shaped-Charge Jets. Simulation was performed using two physicomathematical models (the model of volume fracture and the model of MHD instability) by numerical solution of quasi-two-dimensional nonstationary problems of the dynamic deformation of a high-gradient, conducting, thermally softening rod with a specified time variation of the total current flowing in the rod.

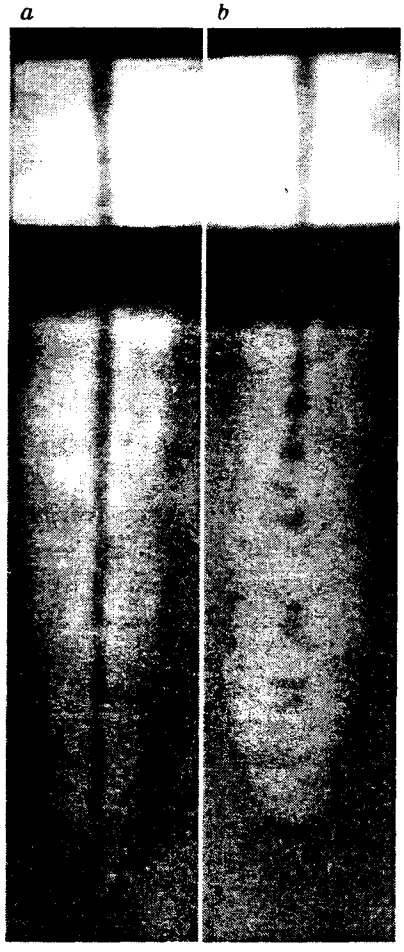

Fig. 2

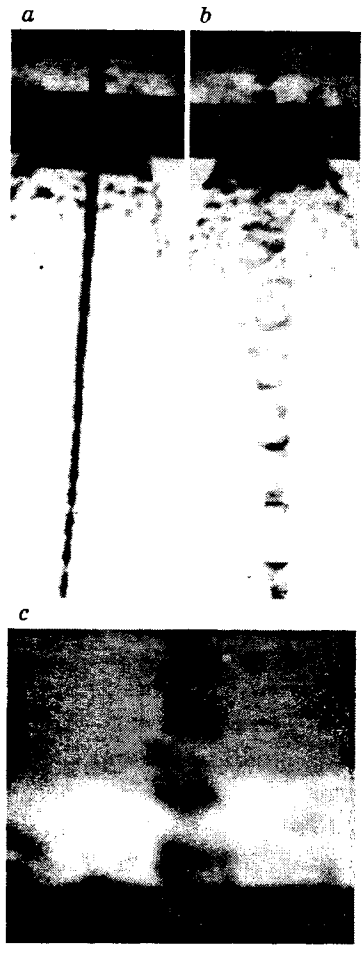

Fig. 3

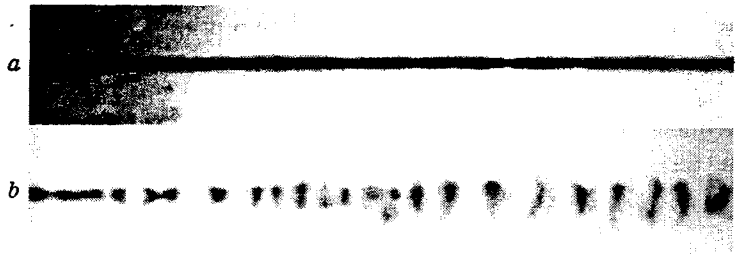

Fig. 4

The volume fracture of the SCJ was studied using the model of a compressed, elastoplastic, cylindrical rod assuming the absence of necking in the SCJ elements [3].

From the numerical calculations by the volume disruption model, it follows that the joint thermal and mechanical effect of the current on the SCJ elements creates conditions for volume fracture of the jet, as a result of which there is radial expansion of the jet material leaving the electrode system. The radial expansion of the jet leads to a decrease in the mean density of the material of the SCJ elements and should influence the penetrability of the jet. Prerequisites for the volume fracture are produced by the considerable heating and thermal softening of the material during motion of the SCJ elements in the interelectrode gap, accompanied by the compressing action of electromagnetic forces. The volume fracture occurs when the SCJ elements leave the interelectrode gap, because of the cessation of the compressing action of electromagnetic

forces, followed by radial unloading and loss of integrity and the ability to resist further deformation. As a result, the material of the SCJ elements disperses in the radial direction with a certain velocity of the outside surface.

The development of MHD instability was studied using a model in which the SCJ elements were regarded as segments of an incompressible, rigid-plastic, axisymmetric rod of variable cross section and volume fracture of the material was ignored. This model assumes that the cross sections are planar, i.e., the jet particles in each cross section have identical axial velocity at any time. This assumption is confirmed by results of a solution of the two-dimensional axisymmetric problem of the deformation of an elastoplastic jet in the absence of any actions [4]. The adopted hypothesis allows one to describe the deformation of the jet within the framework of the one-dimensional problem. The current density j in the model considered was assumed to be distributed uniformly in the cross sections, and the force action of the current was taken into account by specifying the magnetic-field pressure.

At the initial time, small harmonic perturbations were specified on the surface of the SCJ elements. The evolution of the perturbations was determined during the solution of the problem. For the case of "purely mechanical" (without a current) natural development of surface perturbations in deforming SCJ, this model yields results similar to those of more complex models [4].

Variations in the parameters of motion and state of the SCJ elements were described by the following system of equations, which express the laws of conservation of momentum, mass, and energy, respectively:

$$\frac{1}{2}\rho_0 R^2 \frac{du_z}{dt} = \frac{\partial}{\partial z}\int_0^R \sigma_z r\,dr + p_m R\frac{\partial R}{\partial z}, \qquad \frac{dR}{dt} = -\frac{1}{2}\frac{\partial u_z}{\partial z}R,$$

$$R^2\rho_0 c\frac{dT}{dt} = 2\int_0^R \eta j^2 r\,dr + 2\int_0^R \sigma_T \dot{\varepsilon}_i r\,dr.$$

Here z and r are the axial and radial coordinates versus which the following parameters vary: the radius of the rod R, the axial velocity u_z, the temperature T, the resistivity η. and the strain-rate intensity $\dot{\varepsilon}_i$. The specific heat c was considered constant. The axial stresses included in the law of conservation of momentum $\sigma_z = \sigma_z(z, r, t)$ were determined from the physical relations for an incompressible rigid-plastic medium taking into account the boundary conditions of the equality of the total stress vector on the lateral surface to the specific surface magnetic pressure force. Thermal softening was allowed for by the dependence of the current value of the yield strength σ_T on the temperature $\sigma_T = \sigma_{T_0}(T_{\text{melt}} - T)/(T_{\text{melt}} - T_0)$, where T_0 and T_{melt} are the initial temperature and the melting point, respectively.

For the quantitative description of the current effect on the SCJ and the development of MHD instability, we introduced the shape factor k_f, the velocity-redistribution coefficient k_u, and the thermal-softening coefficient k_σ.

The shape factor characterizes the deviation of the shape of an SCJ element from a typical cylindrical shape of a uniformly stretching element of length l_p and radius R_p: $k_f = l/l_p$, where l is a certain effective length determined from the condition $lR_m^2 = l_p R_p^2$, where $R_m = \int R^3(z)\,dz \Big/ \int R^2(z)\,dz$ is the mass-average radius. For an individual SCJ element produced by natural plastic fracture of the jet, the effective shape factor is $k_{fe} \approx 0.6$. For jet elements with a current, the shape factor decreases with increase in the degree of disk formation, and in the limit, it tends to zero. The shape factor k_f allows one to determine the effective length of an SCJ element in the calculation of the SCJ penetration under the action of an electric current. To this end, it is possible to introduce the so-called effective length factor $k_l = 1$ for $k_f \geqslant k_{fe}$ and $k_l = k_f/k_{fe}$ for $k_f \leqslant k_{fe}$.

The velocity-redistribution coefficient

$$k_u = \dot{\varepsilon}_{zm}/\dot{\varepsilon}_{zp},$$

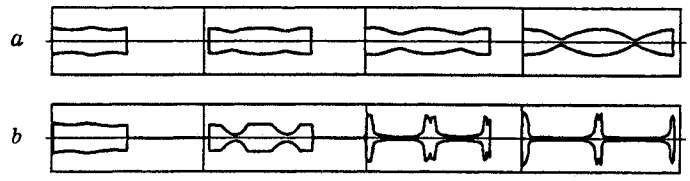

Fig. 5

TABLE 1

I_{max}, kA	t_{max}, μsec	h, mm				
		Experiment	Volume disruption	MHD instability (Δ)	MHD instability (cavern)	MHD instability and volume fracture
250	80	195	200 (+3)	200 (+3)	150 (−23)	200 (+3)
300	40	160	200 (+25)	200 (+25)	131 (−18)	200 (+25)
360	30	147	184 (+25)	200 (+36)	100 (−32)	200 (+36)
350	16	91	132 (+45)	200 (+120)	65 (−29)	98 (+8)
440	17	79	82 (+4)	160 (+103)	54 (−32)	82 (+4)

where

$$\dot{\varepsilon}_{zm} = \int \dot{\varepsilon}_z R^2(z)\,dz \Big/ \int R^2(z)\,dz$$

is the mass-average axial-velocity gradient and $\dot{\varepsilon}_{zp}$ is the axial-velocity gradient for a uniformly stretched element, characterizes the redistribution of the axial velocity along the length of the SCJ element compared to the case of uniform stretching. In the case of a naturally deforming SCJ, the coefficient k_u thus introduced decreases during stretching of the element and reaches a value $k_u = 0$ at the moment of plastic fracture and formation of a separate nongradient element. Under the action of a high current pulse, the factor k_u can take negative values. This indicates that the velocity distribution is inverted and a considerable portion of the material of the element begins to deform under axial compression conditions.

Finally, the thermal-softening coefficient k_σ characterizes the thermal action of the current and is defined as the ratio of the mass-average yield strength of the material to the initial value:

$$k_\sigma = \int \sigma_T R^2(z)\,dz \Big/ \Big[\sigma_{T_0} \int R^2(z)\,dz\Big].$$

This coefficient varies from 1 to 0, assuming the value $k_\sigma = 0$ when the material reaches the melting point.

Calculations show that the electric current not only accelerates the development of the natural instability on the SCJ, leading to its fast disintegration, but at sufficient intensity, it can cause disk formation. This follows from the calculation results in Fig. 5 for the natural deformation of an element of the middle part of an SCJ from a 50-mm SC (Fig. 5a) and the deformation of the same element exposed to a current of 400 kA for 5 μsec (Fig. 5b). Disk formation results from the redistribution of the axial and radial velocities along the length of the element due to the axial compression of the material at the initially small jet necks and an increase in the radius of the bulges. In this case, the elements assume the shape of a thin disk. We note that the disk-formation pattern obtained in the calculations is in fair agreement with the experimental pattern.

Calculations show that the MHD instability occurs at almost the same electric-pulse parameters as volume fracture does. Results of the experiments and calculations of cavern depths in steel and aluminum targets using the models described in the present paper are given in Tables 1 and 2, respectively. The experiments were performed by the diagram shown in Fig. 1b. The data in the plots of I_{max} and t_{max} correspond to the maximum currents and the maximum times when these currents are attained.

The control penetration depths h_0 in experiments without a current in steel and aluminum targets are equal to (205±10) and (365±10) mm, respectively. In Tables 1 and 2, the differences (in percent) between the

TABLE 2

I_{max}, kA	t_{max}, μsec	h, mm			
		Experiment	Volume fraction	MHD instability (cavern)	MHD instability and volume fracture
174	34	257	353 (+37)	257 (0)	330 (+28)
227	19	130	353 (+172)	158 (+21)	335 (+158)
366	22	92	164 (+78)	90 (−2)	144 (+57)
430	23	93	176 (+89)	91 (−2)	156 (+68)

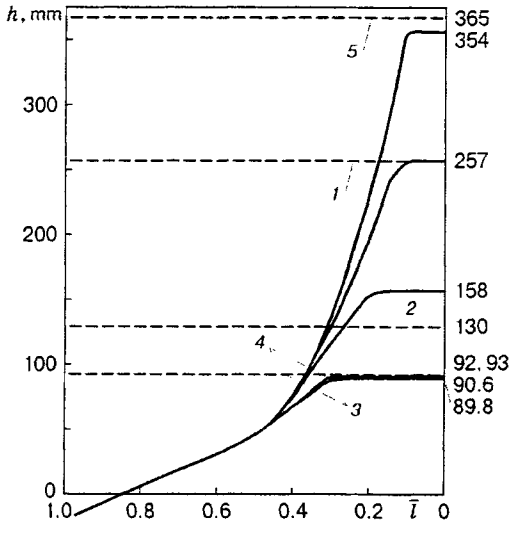

Fig. 6

calculated penetration depths h and the experimental values are given in parentheses for the corresponding models of SCJ disruption. The data in the column "MHD instability (Δ)" agree with the assumption that MHD instability develops in the electrode system (Δ is the electrode separation). The column "MHD instability (cavern)" gives results obtained under the assumption that MHD instability develops both in the electrode gap and in the cavern before the SCJ elements strike the bottom (Fig. 2b).

Figure 6 gives experimental (dashed curves) and calculated (solid curves) values of the cavern depths h in the aluminum target versus the relative length of the generator of the cone $\bar{l}$ ($\bar{l}$ is the ratio of the current length of the generator of the cone to the initial length) obtained on the assumption that the electric current flows through the jet during the entire penetration time. The experiments were performed by the diagram shown in Fig. 1b. Curves 1–4 in Fig. 6 correspond to experimental values h = 257, 130, 92, and 93 from Table 2. Curves 5 correspond to the calculation and experiment with no current in the jet.

Conclusions. The experiments performed show that passage of a current through an SCJ leads not only to the development of necking MHD instability but also to volume fracture of the SCJ when the SCJ elements leave the electrode system. As follows from the calculations, the occurrence of a particular mechanism of SCJ disruption with passage of an electric current depends on the experimental conditions, the electric-pulse parameters, and the time during which the current is passed through the SCJ.

For the steel target, the numerical and experimental results for SCJ penetration agree better with simultaneous allowance for the two mechanisms of SCJ disruption — MHD instability and volume fracture. For the aluminum target, better agreement is achieved under the assumption that only MHD instability develops and the current continues to flow through the jet during jet propagation inside the cavern.

REFERENCES

1. G. A. Shvetsov, A. D. Matrosov, and A. I. Pavlovskii, "Current instability of shaped-charge jets," in: *Proc. of the 10th Pulsed Power Conf.*, Albuquerque, July 3–6 (1995), pp. 1136–1141.
2. G. A. Shevtsov and A. D. Matrosov, "Experimental studies of the current instability of shaped-charge jets," in: *Megagauss and Megaampere Pulsed Technology and Applications*: Proc. VIIth Int. Conf. on Megagauss Magnetic-Field Generation and Related Topics, Inst. of Experimental Phys., Sarov (1997), pp. 979–986.
3. A. V. Babkin, V. A. Kruzhkov, S. V. Ladov, et al., "Behavior of metallic jets under the action of a current pulse," *ibid.*, pp. 992–997.
4. P. C. Chou and J. Carleone, "The stability of shaped-charge jets," *J. Appl. Phys.*, **48**, No. 10, 4187–4194 (1977).